^{10}C + α elastic scattering: A study of the proton-rich ^{14}O nucleus and α clustering

N. R. Ma,[1,2,*] M. Sferrazza,[3] H. Yamaguchi,[1] S. Okamoto,[4] P. Descouvemont,[5] S. Hayakawa,[1] S. Cherubini,[6] T. Doi,[4] Y. Fujikawa,[7] K. Inaba,[7,†] T. Kawabata,[8] A. Kohda,[9] G. Manicò,[6] M. La Cognata,[6] S. Palmerini,[10,11] R. G. Pizzone,[6] A. Sakaue,[7,‡] K. Sakanashi,[8] and H. Shimizu[1]

[1]*Center for Nuclear Study, University of Tokyo, Wako branch, 2-1 Hirosawa, Wako, Saitama 351-0198, Japan*
[2]*Department of Nuclear Physics, China Institute of Atomic Energy, Beijing 102413, China*
[3]*Département de Physique, Université Libre de Bruxelles (ULB), 1050 Brussels, Belgium*
[4]*Department of Physics, Kyoto University, Kita-Shirakawa-Oiwake, Sakyo, Kyoto 606-8502, Japan*
[5]*Physique Nucléaire Théorique et Physique Mathématique, Université Libre de Bruxelles (ULB), 1050 Brussels, Belgium*
[6]*INFN-LNS and Dipartimento di Fisica e Astronomia "E. Majorana", University of Catania, Via S. Sofia 62, 95125 Catania, Italy*
[7]*Department of Physics, Kyoto University, Kita-Shirakawa-Oiwake, Sakyo, Kyoto 606-8502, Japan*
[8]*Department of Physics, Osaka University, 1-1 Machikaneyama-cho, Toyonaka, Osaka 560-0043, Japan*
[9]*Research Center for Nuclear Physics, Osaka University, 10-1 Mihogaoka, Ibaraki, Osaka 567-0047, Japan*
[10]*Dipartimento di Fisica e Geologia, Università degli Studi di Perugia, Via A. Pscoli, 06123 Perugia, Italy*
[11]*INFN Sezione di Perugia, Via A. Pascoli, 06123 Perugia, Italy*

(Received 11 December 2023; revised 10 March 2024; accepted 11 April 2024; published 2 May 2024)

The ^{10}C +α elastic cross section was measured to investigate the structure of the proton-rich ^{14}O nucleus. A radioactive beam of ^{10}C was produced at the RI beam separator CRIB using the ^{10}B(p, n) ^{10}C reaction with a ^{10}B beam energy of 6.99 MeV/nucleon. A complex resonant structure is observed in ^{14}O in the excitation energy region around 13–18 MeV, improving significantly our knowledge on the structure of this nucleus. An R-matrix analysis was performed to determine the properties of resonances. α clustering structure is observed for $J = 0^+$ and $J = 2^+$ at 13.44 and 14.88 MeV, respectively. These results are compared with the α clustering structure reported in the mirror nucleus ^{14}C.

DOI: 10.1103/PhysRevC.109.054302

I. INTRODUCTION

Exotic nuclei have low nucleon (neutron or proton) separation energies leading to unusual properties, such as a large radius [1] or low dipole excitation energies [2]. Advances in the development of radioactive beams [3,4] provide a unique opportunity to improve our knowledge of nuclear properties in extreme conditions approaching the drip lines (shell evolution as a function of the proton/neutron number and the nucleon-nucleon interaction [5], halo structure [6], α clustering [7], dipole strengths [2], etc.).

The proton-rich ^{14}O nucleus is, in general, less known than its mirror nucleus ^{14}C. Some resonances are known up to an excitation energy of 10 MeV with spins and parities assigned [8], but the higher part of the spectrum is not well established. Few resonances are reported without spin assignment, with the 11.97 MeV resonance proposed as a multiplet [8].

The ^{14}O nucleus, moreover, may present an interesting α cluster structure similarly to that observed in ^{14}C [9]. α clustering is a well-known effect in light nuclei. Owing to its high binding energy, the α particle tends to keep its identity in the nucleus. This phenomenon is most likely expected to occur near the α breakup threshold, where the α particle is weakly bound or even slightly unbound. This picture is similar to the description of α radioactivity, and was illustrated, 50 years ago, by the famous Ikeda diagram [10].

Cluster states are characterized by large amplitudes of the wave functions at large distances (large root mean square radii). The most direct method to observe cluster states in a nucleus A is to measure the $\alpha + (A - 4)$ elastic scattering. Elastic cross sections provide information on resonance properties: angular momentum ℓ, energy E_r, and width Γ. From the measured width, one may define the reduced width as $\gamma^2 = \Gamma/2P_\ell(E_r)$, where P_ℓ is the penetration factor in partial wave ℓ [11]. In this way, the strong energy dependence of the total width Γ is removed, and the reduced width provides information on the cluster structure. Traditionally, one uses the dimensionless reduced width θ^2 given by $\theta^2 = \gamma^2/\gamma_W^2$, where the Wigner limit is defined as $\gamma_W^2 = 3\hbar^2/2\mu a^2$ (where μ is the reduced mass and a a typical radius). Cluster states are characterized by a significant fraction of the Wigner limit ($\theta^2 \approx 0.1$–0.5), whereas compact states present smaller θ^2 values (typically $\theta^2 \lesssim 0.05$).

Considering ^{14}C, the mirror nucleus of ^{14}O, a ^{10}Be +α scattering measurement [9] performed at the CRIB (CNS

*mananru@ciae.ac.cn
†Present address: Institute for Advanced Synchrotron Light Source, National Institute for Quantum Science and Technology, 6-6 Aramaki Aoba, Aoba, Sendai, Miyagi 311-0193, Japan.
‡Present address: Center for Nuclear Study, University of Tokyo, Wako branch, 2-1 Hirosawa, Wako, Saitama 351-0198, Japan.

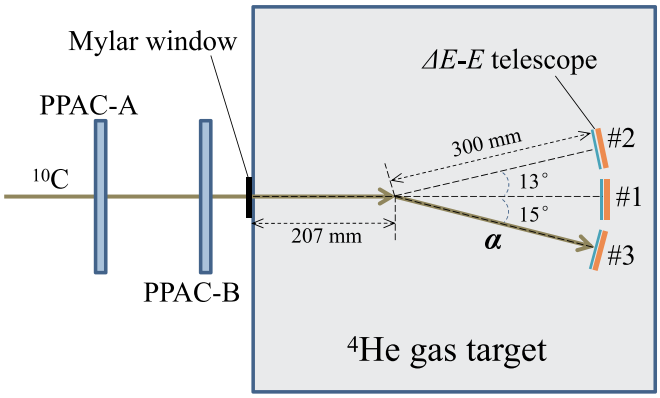

FIG. 1. A schematic of the experimental setup for the $^{10}C+\alpha$ elastic scattering measurement. The distance between detector no. 1 and the mylar window was 507 mm. In the figure the relevant distances are indicated in relation to a reference point. The telescope numbers referred to in the text are also indicated (nos. 1, 2, and 3).

Radioactive Isotope Beam separator) facility of the Center for Nuclear Study, the University of Tokyo [12–14] showed clear evidence of α clustering: three resonances (0^+, 2^+, and 4^+) have large reduced widths and an energy spacing in agreement with a nuclear-cluster band prediction for ^{14}C [9,15–17]. A similar conclusion but with a conflicting result in relation to the linear band head was recently reported by [18].

In the present work, we study the $^{10}C+\alpha$ elastic scattering with two main goals: to investigate the structure of the ^{14}O nucleus (in the energy range of 13–18 MeV) and to explore the possibility of resonances with α cluster structures. The paper is organized as follows. In Sec. II, we describe the experimental setup, and in Sec. III the resulting cross sections are presented. The data are analyzed within the *R*-matrix framework and the results are presented in Sec. IV, together with a comparison with previous works. Section V discusses the α cluster structure for two resonances. The conclusion and outlook are summarized in Sec. VI.

II. EXPERIMENTAL SETUP

The measurement of $^{10}C+\alpha$ elastic scattering was performed using the thick-target inverse kinematics method [19] and a low-energy ^{10}C radioactive beam produced at CRIB. The experimental setup was similar to the one employed in previous works [9]. The $^{10}B(p, n)^{10}C$ reaction in inverse kinematics was used to produce the ^{10}C beam with a ^{10}B primary beam accelerated at 6.99 MeV/nucleon by the RIKEN AVF cyclotron, bombarding a 1.3-mg/ cm^2 -thick cryogenic hydrogen gas target. The ^{10}C beam, after the purification with a Wien filter, had an intensity of 4.3×10^4 particles per second and a beam purity better than 99%.

A schematic of the experimental setup for the elastic scattering is shown in Fig. 1. First, the ^{10}C beam was tracked by two parallel plate avalanche counters (PPAC) [20] (PPAC-A and PPAC-B as shown in Fig. 1), and then it irradiated the ^4He gas target contained in a chamber, where the helium gas pressure was 650 Torr and a 25-μm thick mylar foil sealed the entrance window of the chamber. The two PPACs provided the time-of-flight information of the beam, which was used to perform an unambiguous event-by-event beam particle identification. The ^{10}C beam energy was 36.1 MeV just after the mylar window, measured by a silicon detector.

To detect the recoiled α particles at forward angles, $\Delta E - E$ silicon detector telescopes were installed in the gas target chamber. As shown in Fig. 1, three silicon telescopes were used in the experiment and they were composed by two silicon strip detectors (Micron Semiconductor, Type W1): the first layer as the ΔE detector was a single-sided silicon strip detector (SSSD) with a nominal thickness of 20 μm and the second layer as the E detector was a double-sided silicon strip detector (DSSD) with a thickness of 500 μm. The effective area of the detectors was 50×50 mm^2, and they were composed of 16 strips on one side with the dimension of the pixels of 3×3 mm^2. The forward laboratory angle θ_{lab} (center-of-mass angle around $\theta_{c.m.} = 180^\circ$) was covered by telescope no. 1 at 0° (see Fig. 1). With this telescope we can clearly observe the $^{10}C+\alpha$ resonances. Two additional telescopes, nos. 2 and 3, were installed for both sides of the beam direction at angles 13° and 15° respectively from a reference point (see Fig. 1 for more details), covering the α particles of larger scattering angles.

The energy of these detectors was calibrated with α beams at various energies, as well as with α sources. Before the experiment, all the ΔE and E detectors were independently calibrated with 3-α sources (^{148}Gd-3148 keV, ^{241}Am-5462 keV, ^{244}Cm-5771 keV) and (^{237}Np-4780 keV, ^{241}Am-5480 keV, ^{244}Cm-5795 keV). Additionally, thin ΔE detectors were calibrated with the 3-α source at large incident angle of 60°, to determine their precise thickness distribution by the energy loss. The ΔE detectors had a nominal thickness of 20 μm and the dead layer thickness was about 0.4 μm, but the effective thickness was found to vary from 18.7 to 23.0 μm, depending on the position. At the end of the experiment, telescope no. 1 was first calibrated with a ^4He beam at seven different energies from 9.59 to 28.66 MeV, then telescope nos. 2 and 3 were moved to the center of the target chamber and calibrated together with the ^4He beam at ten energies from 6.32 MeV to 28.71 MeV. At some energy points, a ^6Li beam was also present and used for the calibration.

The $\Delta E - E$ particle identification (PID) plot measured with telescope no. 1 at 0° is shown in Fig. 2: the plot clearly separates protons and α particles. The telescope effectively measured the elastic-scattered α particles in a wide energy range corresponding to $E_{ex} = 12.5$ –20.0 MeV. Figure 2 shows also the protons detected, clearly separated from α particles. Some of them could be from the $^{10}C(\alpha, p)^{13}N$ reaction, and also from the elastic scattering at the entrance of the mylar window, but due to the limited thickness of the E detector, higher energy protons (>8 MeV) penetrated both layers of the telescope and their energies were not correctly measured.

In total, 1.86×10^{10} ^{10}C particles were injected into the gas target as valid events. The ^{10}C beam particles incident on the target were identified with the time-of-flight measurement with the PPACs, and the scattering α particles were selected from the $\Delta E - E$ spectrum. By taking the coincidence events of a ^{10}C particle detected at the PPACs and an α particle hitting on a telescope, the genuine scattering events were

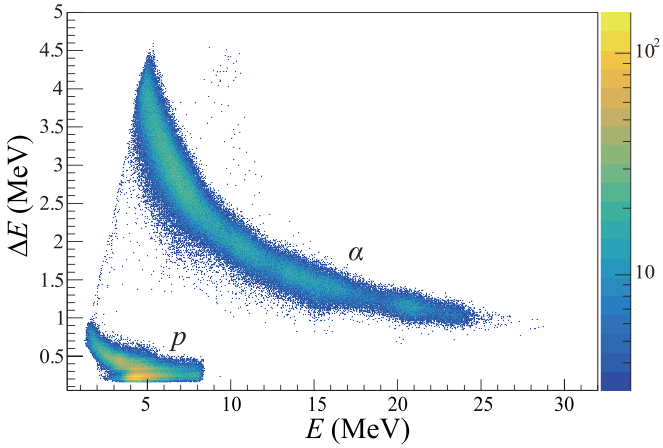

FIG. 2. $\Delta E - E$ particle identification plot measured with telescope no. 1 ($\theta_{\rm lab} = 0{-}8^\circ$). The scattered protons and α particles are clearly separated and identified.

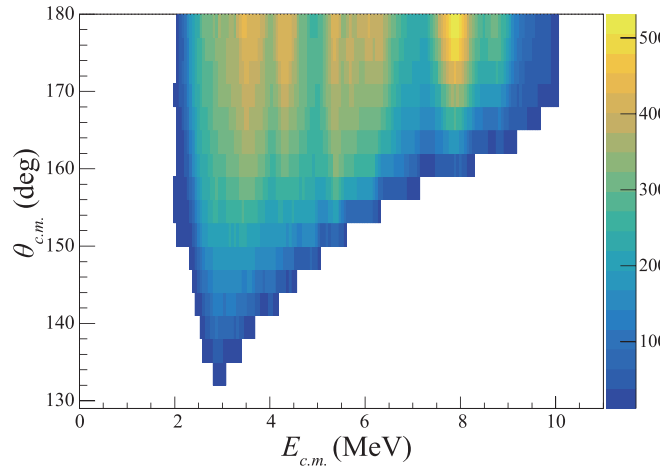

FIG. 3. Energy ($E_{\rm c.m.}$) vs the angular ($\theta_{\rm c.m.}$) distribution of the ^{10}C +α scattering measured by telescope no. 1.

selected. By kinematic reconstruction on an event-by-event basis, the scattering position, the scattering angle $\theta_{\rm lab}$ and the center-of-mass energy $E_{\rm c.m.}$ were determined. After applying proper timing and position cuts, the differential cross section $(d\sigma/d\Omega)_{\rm c.m.}$ (DCS) was calculated from the number of incident ^{10}C particles, the effective target thickness and the solid angle of the detector.

The energy resolution on $E_{\rm c.m.}$ was about 85–115 keV. This resolution is composed of two terms: the energy resolution of the detector (55–90 keV) and the energy straggling of both ^{10}C beam and scattered α particles (40–60 keV). The DCS at large scattering angles was calculated using the elastic scattering events detected in telescope nos. 2 and 3. We note that the DCS has a larger energy uncertainty at larger angles due to the energy straggling and to the angular resolution—1.25° at the lowest $E_{\rm c.m.}$ and better at higher energies—in the reconstruction process.

III. EXPERIMENTAL CROSS SECTIONS

Figure 3 shows the excitation function for telescope no. 1, $E_{\rm c.m.}$ as a function of angular range. In Fig. 3 the peak structures at several fixed energies are visible, which validates the correctness of the kinematics calculation. In particular, resonant scattering peaks near $E_{\rm c.m.}$ = 3.3, 4.2, 5.4, 6.3, and 7.9 MeV ($E_{\rm ex}$ = 13.4, 14.3, 15.4, 16.4, and 18.0 MeV) are observed. The same plots for telescopes nos. 2 and 3 are shown in Fig. 4. The angular dependence of the DCS may reflect the spin value for the resonances: the peaks near $E_{\rm c.m.}$ = 3.3 and 5.4 MeV ($E_{\rm ex}$ = 13.4, 15.4, and 18.0 MeV) are retained to the lower $\theta_{\rm c.m.}$ as in Fig. 4, suggesting that they are from low-spin resonances. On the other hand, the peaks near $E_{\rm c.m.}$ = 4.2, 6.3, and 7.9 MeV ($E_{\rm ex}$ = 14.3, 16.4, and 18.0 MeV) attenuate rapidly with a decreasing of $\theta_{\rm c.m.}$ suggesting that the spins of the resonances around these energies are higher ($J > 3$). The excitation functions segmented into three angular ranges, $\theta_{\rm c.m.}$= 169.1°−172.8°, 172.8°−176.4°, and 176.4°−180° from top to bottom, are shown in Fig. 5. The low-energy part of the spectrum ($E_{\rm c.m.} < 2$ MeV, $E_{\rm ex} < 12.9$ MeV) is rather close to the energy threshold of the detection system and the detection efficiency is uncertain, and thus the points below 2 MeV were excluded from the analysis. The spectrum also has a sharp edge at the highest energy, exactly corresponding to the scattering energy at the target entrance.

In Fig. 3 we observe well-defined vertical straight patterns clearly indicating that the elastic scattering kinematics applied in the analysis of the data was correct. If a considerable contribution of the inelastic scattering would be present, we should expect the straight patterns of Fig. 3 to be bent

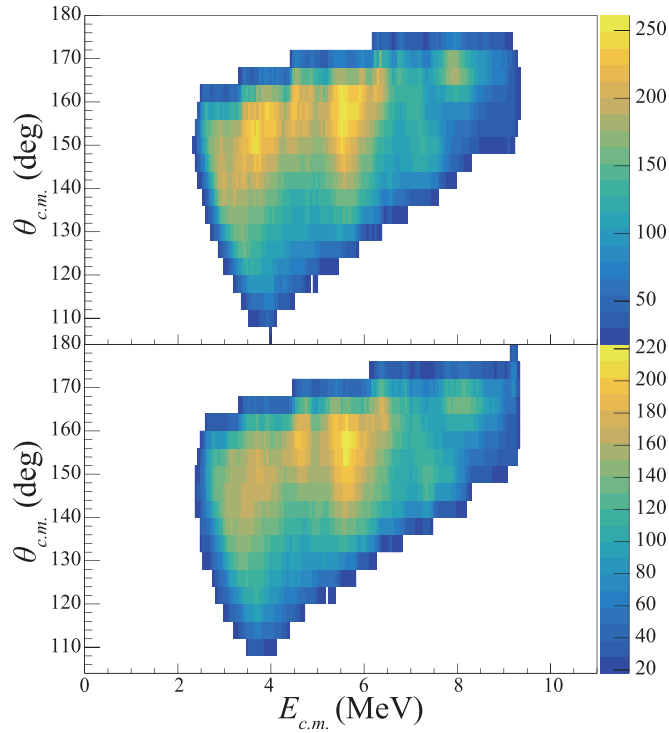

FIG. 4. Energy ($E_{\rm c.m.}$) vs angular ($\theta_{\rm c.m.}$) distributions of the ^{10}C +α scattering measured by the telescope nos. 2 (top) and 3 (bottom).

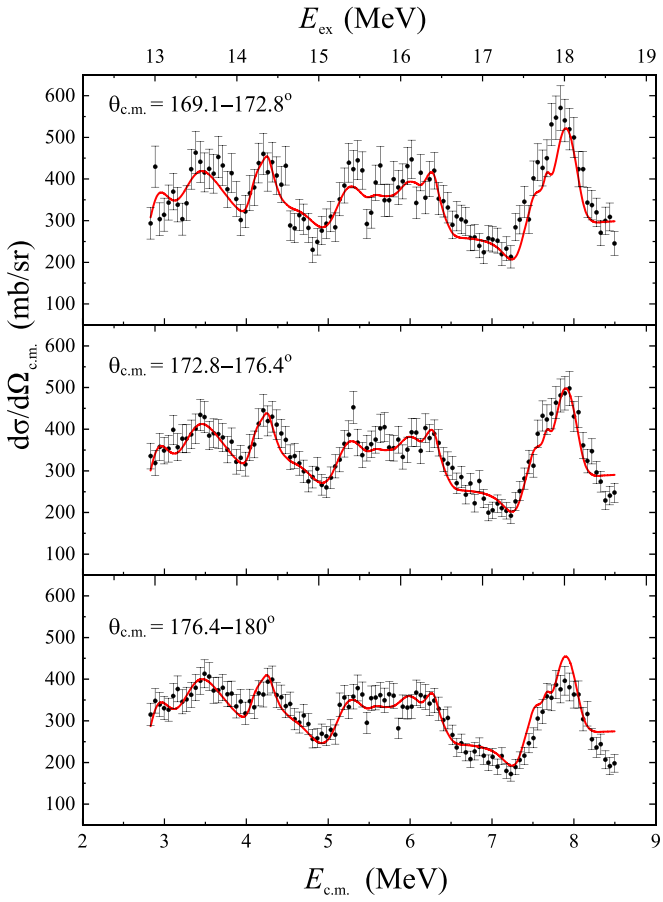

FIG. 5. Experimental center-of-mass cross section of the $^{10}C+\alpha$ scattering $(d\sigma/d\Omega)_{c.m.}$ as a function of $E_{c.m.}$ in the bottom axis and as a function of the excitation energy E_{ex} in the top axis. The DSC data are fitted with the R-matrix calculation using AZURE2 (lines are the fits, $\chi^2/\text{ndof} = 337/291$). From top to bottom $\theta_{c.m.} = 169.1°-172.8°$, $172.8° - 176.4°$ and $176.4°-180°$ respectively.

according to the angle (the so-called the "inelastic shift"), as illustrated in [21]. While the inelastic scattering events may push up the baseline to some extent at the lower energy part of the spectrum, the effect on the deduction of the resonance parameters should be limited. In a similar measurement of the reaction $^{15}O+\alpha$ [22], no evident inelastic scattering was observed in the data, using the time-of-flight information. Moreover, for a previous study of $^{7}Be+\alpha$ [23], NaI detectors were used to identify the inelastic component. It was observed that the inelastic events only produce a small background of around 10% of the elastic scattering, in spite of the low first excitation energy of ^{7}Be (429 keV). Considering the higher first excitation energy for ^{10}C than ^{7}Be, the inelastic scattering is expected to be even smaller in the present case. Based on all these factors, we have assumed the inelastic component does not significantly change our analysis on the resonances and it was neglected.

IV. *R*-MATRIX ANALYSIS

The excitation functions present a complex structure with various resonances (see Fig. 5). We have performed an *R*-matrix analysis [11] for the experimental data with the AZURE2 code [24,25] in order to determine the resonance parameters: energy E_{ex}, spin J, parity π, and width Γ_α. The error analysis of all parameters was also completed by MINOS error analysis function of AZURE2. A typical channel radius of 5.0 fm was used, and small variations around this value provide similar results. The calculated spectrum was broadened with the experimental resolution stated above.

We started the analysis by considering the previous information available in literature in the energy region of our experiment. Only a few resonances are known in the energy region E_{ex}=13–18 MeV; for two resonances, spins and parities have been proposed (see the discussion below). Previous work reported the resonances at 12.84, 13.01 14.15, 14.64, and 17.4 MeV using the $^{14}N(^{3}He, t)\,^{14}O$ reaction with no spins assigned [8]. With two-proton stripping reaction $^{12}C(^{12}C, ^{10}Be)\,^{14}O$, four resonances were reported in ^{14}O: 6.27, 9.9, 14.1, and 15.7 MeV, with tentative spin assignments of (4^+) and (5^-) for the resonances at 14.1 and 15.7 MeV, respectively. The authors indicate the uncertainty of these spin assignments since the shape of the angular distributions of the cross section for these levels do not show an expected spin dependence [26]. The differential cross section for ^{14}O was also measured in the reaction $^{13}C(p, \pi^-)\,^{14}O$ using a proton beam at 100 MeV, and one strong level has been observed at 14.15 MeV for which a possible spin of (5^-) was suggested [27,28]. Other levels were also reported at 14.6 and 17.4 MeV [27,28].

The present experiment, however, indicates the presence of more resonances than the ones reported in literature in this energy range. In order to constrain the parameters, we have fitted the three angular ranges simultaneously. The best fit is shown for the three segments in Fig. 5 and the resonance parameters are reported in Table I. A detailed discussion on the present *R*-matrix analysis for separated energy regions is as follows:

E_{ex} = 12.9–14 MeV. This region presents a broad peak around 13.5 MeV and a weaker one at energy just lower than 13 MeV. The lower part of the spectrum is cut by the acceptance of the present measurement. The weak angular dependence of the spectral shape strongly suggests that this part mainly consists of low-spin resonances. The *R*-matrix analysis indicates a doublet of $1^-/0^+$ at E_{ex}= 12.94 and 13.47 MeV, respectively. Other combinations of doublets with higher spins ($J \geqslant 2$) do not reproduce the data. For example, the introduction of a 2^+ resonance produces a sharper peak, inconsistent with the present broad profile. The previous information obtained with the $^{14}N(^{3}He, t)\,^{14}O$ reaction suggests two resonances at 12.84(5) MeV and 13.01(5) MeV with no spin assignment [8].

E_{ex} = 14–15 MeV. In this region a previous work indicated a 14.15(4) MeV resonance with a spin assignment of (5^-), and another level at 14.64(6) MeV with no spin reported [27,28]. A resonance with $(J^\pi = 4^+)$ was also suggested for the 14.1 MeV state [26]. In the present work, the spectrum in this region presents a clear single peak with an asymmetric shape. We started the *R*-matrix analysis considering the suggested resonances in previous publications in this energy range and we inserted the 5^- level at around 14.2 MeV

TABLE I. Resonance parameters in ^{14}O determined in the present work—$E_{\text{c.m.}}$, E_{ex}, J^π, Γ_α. The table also reports the dimensionless widths θ_α^2. The errors on the level energy derived from the fits are in general very small from the AZURE2 fit, less than 1%. The energy resolution has a value between 85–115 keV as mentioned in the text.

Experimental results					Literature	
$E_{\text{c.m.}}$ MeV	E_{ex} MeV	J^π	Γ_α keV	θ_α^2	E_{ex} MeV	J^π
2.82	12.94	1^-	252 (44)	39.3%	12.84 (5)[a]	
3.32	13.43	0^+	511 (143)	36.4%	13.01 (5)[a]	
4.18	14.29	4^+	6 (2)	3.6%	14.1 [b]/14.15 (4)[c]	(4^+)[b]/(5^-)[c]
4.77	14.88	2^+	385 (296)	23.0%	14.64 (6) [a]	
5.21	15.33	(0^+)	295 (191)	9.7%		
5.56	15.68	(1^-)	8 (7)	0.3%	15.7[d]	(5^-)[d]
6.06	16.17	(3^-)	13 (6)	0.7%		
6.26	16.38	(4^+)	7 (2)	0.7%		
7.41	17.52	1^-	61 (33)	1.5%	17.40 (6)[a]	
7.56	17.68	(5^-)	1 (5)[e]	0.1%		
7.93	18.05	4^+	11 (3)	0.6%		

[a]See [8].
[b]Kraus *et al.* propose a resonance at 14.1 MeV with a possible spin (4^+) [26].
[c]Korkmaz *et al.* propose a spin (5^-) for a resonance at 14.15 MeV [28].
[d]A level at 15.7 MeV is reported with a tentative spin of (5^-) by Kraush *et al.* [26].
[e]The error on Γ_α for this resonance is very large in comparison also to the value: this suggests the important incertitude on this level and the strong correlation with the doublet. However, this resonance is needed to reproduce the data.

[27,28]. However, it was impossible to obtain a reasonable fit of the experimental data using a resonance with this spin. The structure is consistent with a 4^+ resonance at 14.29 MeV, in agreement with the previous tentative spin assignment for the 14.1 MeV state [26]. We tried to fit the data using a different spin other than the 4^+, however, none of them could reproduce the unique peak shape of this isolated resonance. Another 2^+ resonance at 14.88 MeV was also introduced in the analysis, as we found it completely reproduces the high energy tail of the peak.

***E*$_{\text{ex}}$ = 15–17 MeV.** This part is complex and appears as a plateau with a finer structure, which certainly needs several resonances to reproduce its shape. The proposed fit includes a 0^+ resonance at 15.33 MeV (the first peak) and a 1^- resonance at 15.68 MeV. The higher energy edge of the plateau has a sharp drop of DCS, and diminishes relatively quickly as $\theta_{\text{c.m.}}$ decreases (also Fig. 4 shows the bump made by these two peaks near the disappearance in the $\theta_{\text{c.m.}} < 150^\circ$ region). The best fit for this behavior has been obtained with two peaks, 3^- and 4^+ at 16.16 and 16.38 MeV, respectively. This part of the spectrum, due to its complex structure, could allow a different possibility for the spin and parity assignments: the shape of the first part of the spectrum was also consistent with a 2^+ at 15.32, and 3^- and 4^+ at 16.16 and 16.38 MeV, respectively. However, this alternative does not reproduce well the data in the region around 15.7 MeV: the present experimental data indicate a peak and are better reproduced by the presence of a doublet of $(1^-, 0^+)$ as reported in Table I. We have also tried to impose a 5^- level around 15.7 MeV as it was suggested in Ref. [26], but failed to obtain a reasonable fit of this region. Due to the complexity of the spectrum, the spin and parity assignments in this region is less firm, even though the proposed fit reproduces well the data for the three angular ranges.

***E*$_{\text{ex}}$ = 17–18.5 MeV.** This part of the spectrum shows a very strong peak around 18 MeV, with the intensity diminishing quickly as $\theta_{\text{c.m.}}$ decreases. It presents a width larger than the experimental resolution, and cannot be well fitted with a single resonance. The peak has a slightly asymmetrical shape, also suggesting the need of several resonances. The best fit for the main peak was obtained with a doublet of 5^- and 4^+ states at 17.68 and 18.05 MeV, respectively. The proposed (5^-) level is, however, not firm and the large uncertainty of the Γ_α could be an indication of the correlation with the other resonance 4^+ in the doublet. Although the width of the (5^-) resonance is small and uncertain, we found that an *R*-matrix calculation without this 5^- resonance induces a large deviation from the experimental data. This indicates the need of two resonances for reproducing this peak. A similar peak was observed in the ^{10}Be +α study [9], where the best fit was obtained also with a doublet of 5^- and 4^+ states. A 1^- resonance at 17.52 MeV was introduced to reproduce the lower part of the spectrum. Information in this energy region by previous works was limited to a resonance of 17.40(6) MeV with no spin assignment.

V. α CLUSTERING IN ^{14}O

The results reported in Table I indicate two levels, the 0^+ and the 2^+ at 13.43 and 14.88 MeV, respectively, with relatively large reduced widths θ_α^2 (36% and 23%). As mentioned in the Introduction, α cluster states have a significant fraction of the Wigner limit ($\theta_\alpha^2 \approx$ 10–50 %), in contrast to compact states that present smaller θ_α^2 values.

The existence of the "linear-chain cluster states", an exotic form of α clustering, has been discussed extensively for ^{14}C and ^{14}O in the recent years with contrasting results [9,15–18,29–31]. Several α-cluster states were observed in the

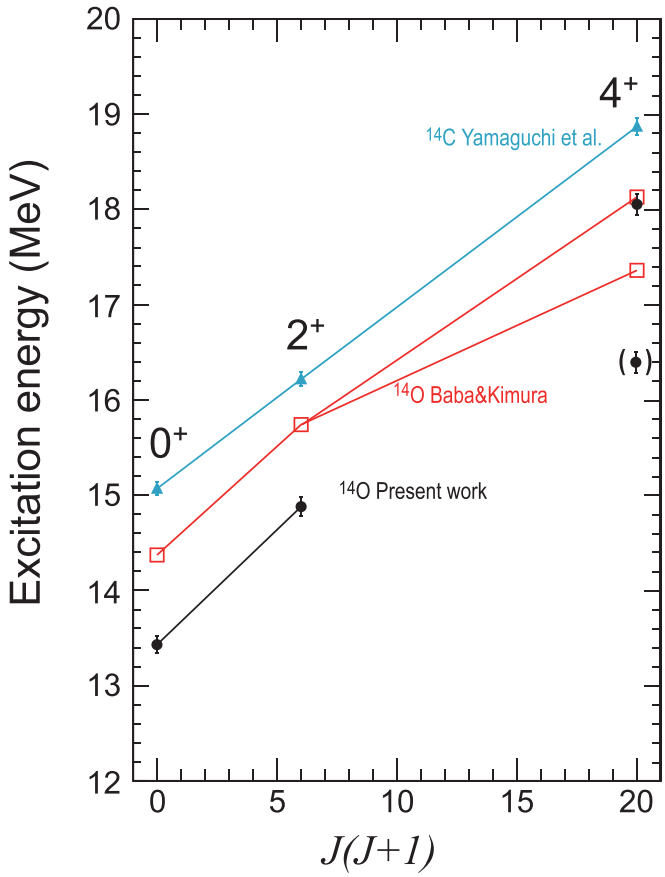

FIG. 6. Excitation energies of the resonances in ^{14}O plotted against $J(J+1)$ for the predicted linear chain band [17] (open square) and by the present work (solid circles). The candidate of the linear-chain band in ^{14}C proposed in [9] is also plotted for comparison (solid triangle). The lower 4^+ state in the present work is with a tentative J^π assignment and plotted with parentheses.

mirror nucleus ^{14}C in a previous measurement of ^{10}Be $+\alpha$ [9], and the authors interpreted the results as a rotational band consistent with a model of this linear-chain cluster state by Suhara and Kanada-En'yo [15,16]. Their observation also indicated, both theoretically and experimentally, that clustering effects decrease when the angular momentum increases. Then, Baba and Kimura [17] performed theoretical calculations to investigate linear-chain states in both ^{14}C and ^{14}O, where "π-bond" linear-chain states were defined as those corresponding to the prediction in [15]. Very recently another work reported on the linear-chain molecular rotational band in ^{14}C with a method to measure the break-up of ^{14}C [18], proposing a different energy of the band head from [9] or [15,16], but rather consistent with [17].

In Fig. 6, the cluster states observed in the present work are compared with the rotational band proposed with the similar resonant-scattering experiment for the mirror system ^{14}C [9], and the theoretical calculation for ^{14}O [17]. This calculation indicated that the $J^\pi = 4^+$ is fragmented into two states at 17.36 and 18.13 MeV as shown in Fig. 6, while the corresponding 4^+ state in ^{14}C stays as a single state. Figure 6 also shows the cluster states in ^{14}O identified in the present work at 13.42 MeV (0^+) and 14.88 MeV (2^+). These energies have offsets of about 1 MeV with respect to the cluster states proposed by [17]. In our R-matrix analysis of ^{14}O, we identified a 4^+ resonance at 18.05 MeV forming a doublet with 5^-, similarly to the doublet observed in ^{14}C [9], as well as another (4^+) at 16.38 MeV. However, both 4^+ have θ_α^2 of around 0.7%, four times smaller than that of the 4^+ state found in the mirror nucleus, 2.4(9)% [9], indicating the non-α-cluster nature for this state. Since the 4^+ cluster state of the rotational band is not observed in the present experimental observation of ^{14}O, the two α-clustering resonances— 0^+ and 2^+ —could have different structural properties compared to the prediction [17] or to the interpretation of the rotational band observed in ^{14}C [9,18]. Further theoretical and experimental works for a more comprehensive understanding would be needed.

VI. CONCLUSIONS

In summary, we studied the structure of the proton-rich nucleus ^{14}O with the resonant elastic scattering ^{10}C $+\alpha$ reaction. A complex structure was observed with many new resonances observed in the energy range of 13–18 MeV. The R-matrix fit allows to determine the properties of the resonances (energy, spin, parity, and width). The results were compared with published data, and some spin assignments are proposed (for example we assign 4^+ for the 14.2 MeV level). α-cluster-like states are proposed for the 0^+ and 2^+ at 13.44 and 14.88 MeV, respectively. A further experimental work is needed for a better understanding of the structure of this nucleus in comparison also with the mirror ^{14}C nucleus. An experimental study of the ^{13}N $+p$ elastic scattering in the same energy region, for example, could provide additional constraints on the R-matrix fit and clarify further the resonance properties of this nucleus, in particular at higher energies.

ACKNOWLEDGMENTS

The work was supported by the Fonds de la Recherche Scientifique - FNRS under Grants No. J.0174.22 and No. 4.45.10.08. The experiment was performed at RI Beam Factory operated by RIKEN Nishina Center and CNS. We thank RIKEN and CNS accelerator staff for the primary beam production and acceleration. This work was partly supported by JSPS KAKENHI (No. 18K13556, No. 19K03883, and No. 23H01181) in Japan and NSFC (No. 12175313) in China. M.S. and H.Y. gratefully acknowledge the financial support from ARES of Belgium via the ASEM-DUO fellowships.

[1] I. Tanihata and B. Jonson, Halo Nuclei, in *Handbook of Nuclear Physics*, edited by I. Tanihata, H. Toki, and T. Kajino (Springer Nature, Singapore, 2023), pp. 985–1026.

[2] T. Nakamura, *Coulomb Breakup and Soft E1 Excitation of Neutron Halo Nuclei*, [1], pp. 1205–1241.

[3] Y. Blumenfeld, T. Nilsson, and P. Van Duppen, Phys. Scr. **T152**, 014023 (2013).

[4] K. Wimmer, J. Phys. G **45**, 033002 (2018).
[5] T. Otsuka, A. Gade, O. Sorlin, T. Suzuki, Toshio, and Y. Utsuno, Rev. Mod. Phys. **92**, 015002 (2020).
[6] P. Descouvemont, Phys. Rev. C **104**, 024613 (2021).
[7] Y. Funaki, H. Horiuchi, and A. Tohsaki, Prog. Part. Nucl. Phys. **82**, 78 (2015).
[8] F. Ajznberg-Selove, Nucl. Phys. A **523**, 1 (1991).
[9] H. Yamaguchi, D. Kahl, S. Hayakawa, Y. Sakaguchi, K. Abe, T. Nakao, T. Suhara, N. Iwasa, A. Kim, D. H. Kim, S. Cha, M. Kwag, J. Lee, E. Lee, K. Chae, Y. Wakabayashi, N. Imai, N. Kitamura, P. Lee, J. Moon *et al.*, Phys. Lett. B **766**, 11 (2017).
[10] K. Ikeda, N. Takigawa, and H. Horiuchi, Prog. Theor. Phys. Suppl. **E68**, 464 (1968).
[11] P. Descouvemont and D. Baye, Rep. Prog. Phys. **73**, 036301 (2010).
[12] S. Kubono, Y. Yanagisawa, T. Teranishi, S. Kato, T. Kishida, S. Michimasa, Y. Ohshiro, S. Shimoura, K. Ue, S. Watanabe, and N. Yamazaki, Eur. Phys. J. A **13**, 217 (2002).
[13] Y. Yanagisawa, S. Kubono, T. Teranishi, K. Ue, S. Michimasa, M. Notani, J. He, Y. Ohshiro, S. Shimoura, S. Watanabe, N. Yamazaki, H. Iwasaki, S. Kato, T. Kishida, T. Morikawa, and Y. Mizoi, Nucl. Instrum. Methods Phys. Res. A **539**, 74 (2005).
[14] H. Yamaguchi, Y. Wakabayashi, G. Amadio, S. Hayakawa, H. Fujikawa, J. H. S. Kubon and, A. Kim, and D. Binh, Nucl. Instrum. Methods Phys. Res. A **589**, 150 (2008).
[15] T. Suhara and Y. Kanada-En'yo, Phys. Rev. C **82**, 044301 (2010).
[16] T. Suhara and Y. Kanada-En'yo, Phys. Rev. C **84**, 024328 (2011).
[17] T. Baba and M. Kimura, Phys. Rev. C **99**, 021303(R) (2019).
[18] J. Han, Y. Ye, J. Lou, X. Yang, Q. Li, Z. Yang, Y. Yang, J. Wang, J. Xu, Y. Ge, H. Hua, Z. Li, B. Yang, Y. Liu, S. Bai, K. Ma, J. Chen, G. Li, Z. Hu, H. Yu *et al.*, Commun. Phys. **6**, 220 (2023).
[19] K. P. Artemov, O. P. Belyanin, A. L. Vetoshkin, R. Wolskj, M. S. Golovkov, V. Z. Goldberg, M. Madeja, V. V. Pankratov, I. N. Serikov, V. A. Timofeev, V. N. Shadrin, and J. Szmider, Sov. J. Nucl. Phys. **52**, 408 (1990).
[20] H. Kumagai, A. Ozawa, N. Fukuda, K. Sümmerer, and I. Tanihata, Nucl. Instrum. Methods Phys. Res. A **470**, 562 (2001).
[21] J. J. He, S. Kubono, T. Teranishi, M. Notani, H. Baba, S. Nishimura, J. Y. Moon, M. Nishimura, H. Iwasaki, Y. Yanagisawa, N. Hokoiwa, M. Kibe, J. H. Lee, S. Kato, Y. Gono, and C. S. Lee, Phys. Rev. C **76**, 055802 (2007).
[22] D. Torresi, C. Wheldon, T. Kokalova, S. Bailey, A. Boiano, C. Boiano, M. Fisichella, M. Mazzocco, C. Parascandolo, D. Pierroutsakou, E. Strano, M. Zadro, M. Cavallaro, S. Cherubini, N. Curtis, A. Di Pietro, J. P. Fernández Garcia, P. Figuera, T. Glodariu, J. Gręboszet *et al.*, Phys. Rev. C **96**, 044317 (2017).
[23] H. Yamaguchi, D. Kahl, Y. Wakabayashi, S. Kubono, T. Hashimoto, S. Hayakawa, T. Kawabata, N. Iwasa, T. Teranishi, Y. K. Kwon, D. N. Binh, L. H. Khiem, and N. N. Duy, Phys. Rev. C **87**, 034303 (2013).
[24] R. E. Azuma, E. Uberseder, E. C. Simpson, C. R. Brune, H. Costantini, R. J. de Boer, J. Görres, M. Heil, P. J. LeBlanc, C. Ugalde, and M. Wiescher, Phys. Rev. C **81**, 045805 (2010).
[25] E. Uberseder and R. J. deBoer, AZURE2 user manual (2015).
[26] L. Kraus, A. Boucenna, I. Linck, B. Lott, R. Rebmeister, N. Schulz, J. C. Sens, M. C. Mermaz, B. Berthier, R. Lucas, J. Gastebois, A. Gillibert, A. Miczaika, E. Tomasi-Gustafsson, and C. Grunberg, Phys. Rev. C **37**, 2529 (1988).
[27] E. Korkmaz, L. C. Bland, W. W. Jacobs, T. G. Throwe, S. E. Vigdor, M. C. Green, P. L. Jolivette, and J. D. Brown, Phys. Rev. Lett. **58**, 104 (1987).
[28] E. Korkmaz, S. E. Vigdor, W. W. Jacobs, T. G. Throwe, L. C. Bland, M. C. Green, P. L. Jolivette, and J. D. Brown, Phys. Rev. C **40**, 813 (1989).
[29] M. Freer, J. D. Malcolm, N. L. Achouri, N. I. Ashwood, D. W. Bardayan, S. M. Brown, W. N. Catford, K. A. Chipps, J. Cizewski, N. Curtis, K. L. Jones, T. Munoz-Britton, S. D. Pain, N. Soić, C. Wheldon, G. L. Wilson, and V. A. Ziman, Phys. Rev. C **90**, 054324 (2014).
[30] A. Fritsch, S. Beceiro-Novo, D. Suzuki, W. Mittig, J. J. Kolata, T. Ahn, D. Bazin, F. D. Becchetti, B. Bucher, Z. Chajecki, X. Fang, M. Febbraro, A. M. Howard, Y. Kanada-En'yo, W. G. Lynch, A. J. Mitchell, M. Ojaruega, A. M. Rogers, A. Shore, T. Suhara *et al.*, Phys. Rev. C **93**, 014321 (2016).
[31] J. Li, Y. L. Ye, Z. H. Li, C. J. Lin, Q. T. Li, Y. C. Ge, J. L. Lou, Z. Y. Tian, W. Jiang, Z. H. Yang, J. Feng, P. J. Li, J. Chen, Q. Liu, H. L. Zang, B. Yang, Y. Zhang, Z. Q. Chen, Y. Liu, X. H. Sun *et al.*, Phys. Rev. C **95**, 021303(R) (2017).